KSME

Springer

Journal of Mechanical Science and Technology 34 (12) 2020

Original Article
DOI 10.1007/s12206-020-1101-8

Keywords:
· Time-varying bearing stiffness
· Multiple clearance
· Nonlinear dynamics
· Meshing beyond pitch point
· Time-varying friction
· Bifurcation
· Lyapunov
· Experiment verification

Correspondence to:
He-yun Bao
baoheyun@nuaa.edu.cn

Citation:
Bao, H., Jin, G., Lu, F. (2020). Nonlinear dynamic analysis of an external gear system with meshing beyond pitch point. Journal of Mechanical Science and Technology 34 (12) (2020) 4951~4963.
http://doi.org/10.1007/s12206-020-1101-8

Received October 29th, 2019
Revised July 25th, 2020
Accepted September 1st, 2020

† Recommended by Editor
No-cheol Park

Nonlinear dynamic analysis of an external gear system with meshing beyond pitch point

He-yun Bao, Guang-hu Jin and Feng-xia Lu

Laboratory of Science and Technology on Helicopter Transmission, Nanjing University of Aeronautics and Astronautics, Nanjing 210016, China

Abstract A two-dimensional non-linear dynamics model of a gear with meshing beyond pitch point with six degrees has been established, considering time-varying meshing stiffness, time-varying bearing stiffness, time-varying friction, backlash and bearing clearance. Time-varying meshing stiffness is computed by using material mechanics method. The friction coefficient of Coulomb model and the friction coefficient of EHL theory are analyzed and compared in dynamic response. The global bifurcation characteristics caused by input speed, backlash, bearing clearance and damping are investigated. The maximum Lyapunov exponent which leads to chaos characters effect of changing parameters is analyzed. The verification experiment is carried out on the CL-100 test rig. Meshing frequency has main impact on vibration acceleration of ordinary spur gear and double meshing frequency has main impact on vibration acceleration of gear with meshing beyond pitch point. The results show that the gear with meshing beyond is better than ordinary spur gear whether in bifurcation characteristics or in vibration acceleration response.

1. Introduction

Gear train plays an important role in the area of mechanical drive, which is widely used in various areas of transmission machinery, such as automobiles, wind engines, marine, aeronautics and astronautics, etc. Lots of literature [1] shows that time-varying meshing stiffness and gear mesh errors lead to vibration. The tooth friction causes vibration of normal to mesh curve, and the changing direction of friction leads to gear system vibration especially in high speed gear transmission. So, it is necessary to study the effect of time-varying tooth friction coefficient. Velex and Sainsot [2] studied an original analytical analysis of tooth friction excitations in error-less spur and helical gears, based on the Coulomb model. Vaishya and Houser [3, 4] established a six-degree model with tooth friction and time-varying mesh stiffness, the effect of tooth friction leading to dynamic of gear system by numerical integration method are studied. Real mesh stiffness is considered and different friction coefficient lubrication model is established [5, 6]. Tang [7] proposed a non-linear dynamic model for gear pair system considering surface friction, gear mesh stiffness and backlash. The dynamic distribution of load in the mesh area was considered in calculating the friction force. He used Buckingham [8] semi-empirical equations to calculate tooth surface friction coefficient. Period enlargement method was used to establish the friction force and gear meshing stiffness models. Zhang [9] established a 6-DOF nonlinear dynamic model for a spur gear with consideration of friction. Benedict & Kelly model is used to calculate time-varying friction coefficient. The realistic time-varying mesh stiffness was calculated, and time-varying friction coefficient was analyzed based on a mixed lubrication model. The gear train systems with various tooth surface roughness, the dynamic responses of the gear meshing, such as nor-mal load, friction force, bearing force and dynamic transmission error (DTE) were comparatively investigated in time and frequency domain with numerical simulation method. Sun [10] studied the calculation of mean friction coefficient in scuffing strength for gear train with drive with meshing beyond pitch point. Li [11] established a nonlin-

ear lateral-torsional coupled vibration model of a planetary gear system considering transmission errors, time varying meshing stiffness and multiple gear backlashes, and analyzed the effect of rotational speed of sun gear on bifurcation. Tang [12] analyzed effect of static transmission error on dynamic responses for spiral bevel gears and solved dynamic response, bifurcation map, time domain response, phase curve and poincare map of the system. The homoclinic bifurcation and transition to chaos in gear systems are studied both analytically and numerically [13]. Chang-Jian and Chang [14] investigated the dynamic responses of a single-degree-of freedom spur gear system with and without nonlinear suspension and found the bifurcation and chaotic dynamics in this system. Li [15] established a nonlinear dynamic model of bending-torsion coupling for gear-rotor-rolling bearing transmission system, considering the gear eccentricity and nonlinear contact of rolling bearing, the influence law of parameters on the system vibration response was analyzed. Sheng and Zhu [16] established a six degree of freedom transverse-torsion coupled nonlinear gear-totor-bearing vibration model with multiple clearance and tooth surface friction, while time-varying meshing stiffness, ear backlashes, bearing clearance were considered in this mode as well. Xiang [17] tested experimental modal of the spiral bevel gear wheel using the PolyMAX method. Chen [18] analyzed dynamic characteristics of a planetary gear system based on contact status of the tooth surface. Yu [19] studied fault diagnosis of planetary gearbox with incomplete information using assignment reduction and flexible naive Bayesian classifier.

A 6-DOF nonlinear dynamic is established in this paper, time-varying tooth friction, backlash and bearing clearance are considered. The friction coefficient model of Coulomb and the EHL theory are analyzed and compared in dynamic response. Time-varying meshing stiffness is computed by using material mechanics method and fitted by Fourier series method. The dynamic equations are solved by 4^{th}-5^{th} variable step Runge-Kutta numerical method. The dynamical behavior of an ordinary gear train and the gear train with meshing beyond pitch point are compared and studied by bifurcation diagram, maximum Lyapunov, phase chart and time domain chart. The verification experiment is carried out on the CL-100 test rig.

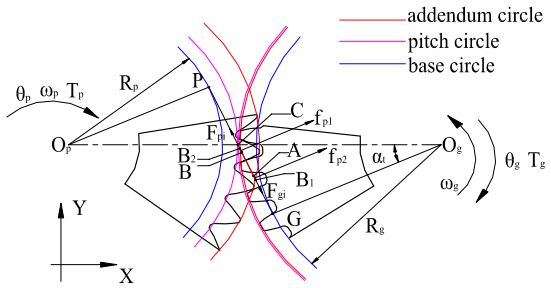

Fig. 1. The GMBP of mesh state and force analysis.

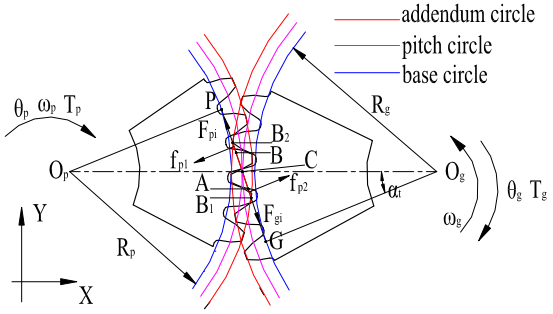

Fig. 2. The OSG of mesh state and force analysis.

2. Dynamic model of system

The gear train with meshing beyond pitch point (GMBP) mesh state and force analysis are showed in Fig. 1 [20], the input gear rotates clockwise around O_P by torque T_P, while the output gear rotates counterclockwise around O_g by load T_g, PG is direction during the meshing. Points B and A are critical theoretical line of action, B2B1 is actual line of action and located in one side of the pitch point, so friction doesn't change points of single and double teeth.

The ordinary spur gears (OSG) of mesh state and force analysis can be found in Fig. 2, the driving gear rotates clockwise around O_P by torque T_P, the driven gear rotates counterclockwise around O_g by load T_g, PG is theoretical line of action, B2B1 is actual line of action and located in both sides of the pitch point, so friction changes direction during the meshing. Points B and A are critical points of single and double teeth.

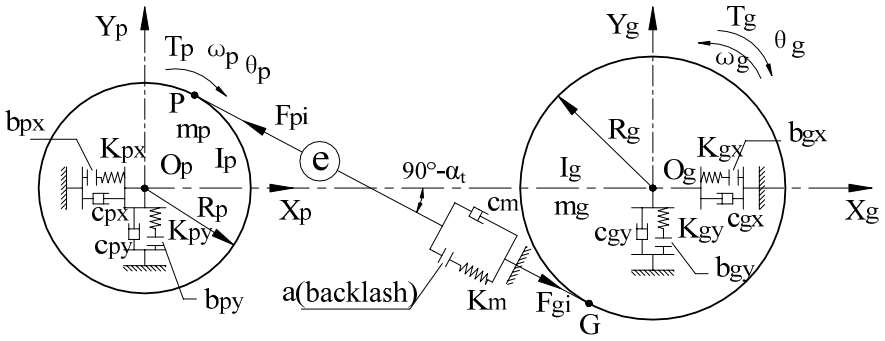

Fig. 3. A 6-DOF nonlinear dynamic model.

Table 1. The parameters of gear train.

Parameter	GMBP (value)	OSG (value)
Module of input gear/ m_1 (mm)	2.8040	2.6915
Module of output gear/ m_2 (mm)	2.6915	2.6915
Number of input teeth/ z_1	30	32
Number of output teeth/ z_2	36	36
Pressure angle of input gear/ α_1(°)	25.8268	20.3259
Pressure angle of output gear/ α_1(°)	20.3259	20.3259
Modification coefficient of input gear/ x_1	0.7606	-0.05
Modification coefficient of output gear/ x_2	-0.6095	0.046
Addendum coefficient/ h_a*	0.8	1
Coefficient of bottom clearance/ c*	0.3	0.25
Tooth width/ B (mm)	20	20
Center distance/a' (mm)	91.5	91.5
Coefficient with meshing beyond pitch point/λ	0.167	/

According to the analysis, a 6-DOF nonlinear dynamic model is established in Fig. 3 with the lamped-parameter method. Where, K_m is time-varying meshing stiffness and c_m is time-varying meshing damping, K_{px}, K_{py}, K_{gx}, K_{gy} represent bearing stiffness, c_{px}, c_{py}, c_{gx}, c_{gy} represent bearing damping, $e(t)$ means that comprehensive error.

3. Parameters of the system

The gear with meshing beyond pitch point (GMBP) requires the following conditions to be satisfied: a) coefficient with meshing beyond pitch point ≥ 0; b) contact ratio ≥ 1; c) addendum thickness ≥ (0.25~0.4)*module; d) gear of meshing hasn't interference; e) meeting strength requirements of bending, contact and bonding. b)-e) are the limiting conditions of ordinary spur gears (OSG). According to above constraints, the gear train system parameters are shown in Table 1.

4. Equations of motion

As the actual mesh line is located in one side of the pitch point, the calculation criterions will not apply for the gear train with meshing beyond pitch point. The teeth are considered as non-homogeneous cantilever beams, the stiffness of the external gears with meshing beyond pitch point considering gear wheel body deformation is computed by using material mechanics method [21]. As time-varying meshing stiffness has periodicity, which is similar with the Fourier series method, as shown in Eq. (1).

$$K_m(t) = k_0 + \sum_{i=1}^{n}(A_{ki\cos}\cos(i\omega t+\varphi) + A_{ki\sin}\sin(i\omega t+\varphi)) \quad (1)$$

where, k_0 is gear pair mesh synthesizing stiffness, ω is meshing frequency, φ is initial phase. The time-varying meshing stiffness are fit by 2nd Fourier series as shown in Fig. 4.

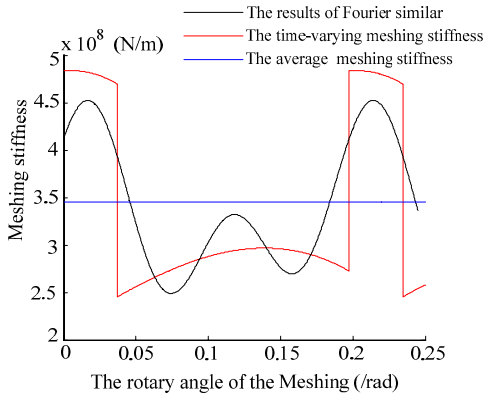

Fig. 4. Time-varying meshing stiffness of GMBP.

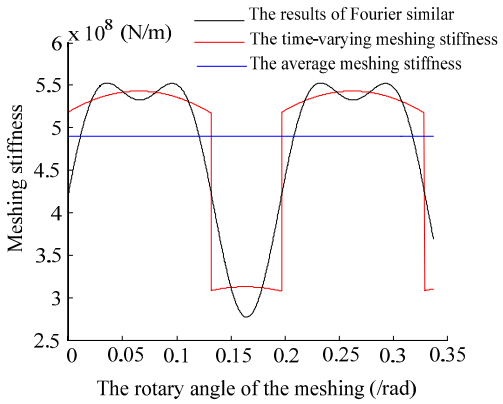

Fig. 5. Time-varying meshing stiffness of OSG.

The time-varying meshing stiffness of ordinary gear is solved by the same method, as shown in Fig. 5.

The load distribution is a variable during meshing, which is solved by stiffness of spur gear and error, as shown in Eq. (2). Every meshing tooth has the same total deformation when

Table 2. The parameters value of EHL model.

Parameter	b1	b2	b3	b4	b5	b6	b7	b8	b9
Value	-8.9164	1.033	1.0360	-0.3540	2.8120	-0.1006	0.7527	-0.3909	0.6203

Table 3. The parameters of condition.

Power (kW)	Input speed (r/min)	Dynamic viscosity of lubricating oil (cPs)	The RMS surface roughness (μm)
200	5000	27.4365	0.06

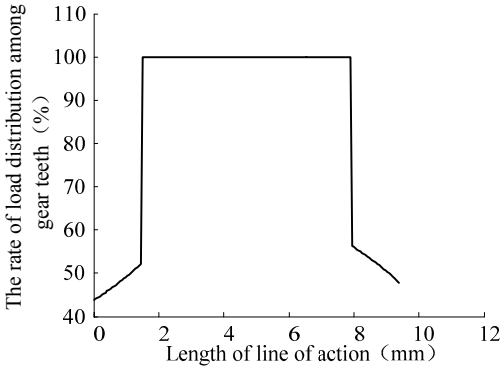

Fig. 6. The rate of load share among gear teeth of GMBP.

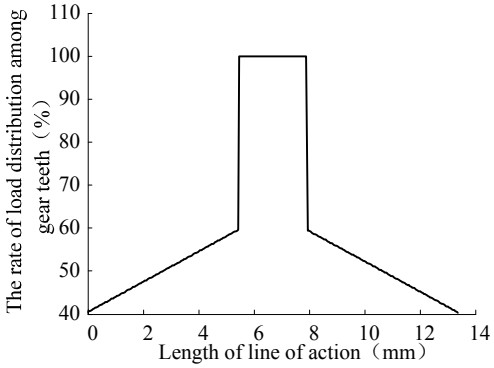

Fig. 7. The rate of load share among gear teeth of OSG.

gear is in double meshing area. Results are shown in Figs. 6 and 7.

$$\frac{F_{AC}}{K_{AC}}+\alpha_1+\gamma_1=\frac{F_{BD}}{K_{BD}}+\alpha_2+\gamma_2 \tag{2}$$

where, F_{AC} and F_{BD} are meshing force, α_1 and α_2 are modified value of meshing point, γ_1 and γ_2 are festival deviation and tooth alignment error, respectively.

Friction coefficient is related to teeth topography, roughness of teeth surface, sliding speed, contact stresses and lubrication. It is studied by Coulomb friction model, Buckingham's empirical formula, Benedict & Kelly's empirical formula and EHL theory at present.

Coulomb model supposes that friction coefficient is a constant value without changing direction in pitch point during the meshing. Calculation formula is shown as Eq. (3).

$$\mu=\mu_0 sign(B_2C-\mathrm{mod}(R_p\omega_p t,P_b)) \tag{3}$$

where, B_2C is distance from start point of meshing to pitch point, R_p is radius of driving gear base circle, P_b is base pitch. Friction may change direction in ordinary spur gear, but actual mesh line is located in one side of the pitch point. μ_0 is a amplitude of friction coefficient, as shown in Eq. (4).

$$\mu_0=0.12(W_tR_a/\eta_m\upsilon_{\Sigma_p}\rho_{red,p})^{0.25} \tag{4}$$

where, R_a is roughness of teeth surface, W_t is tangent load of unit tooth width, η_m is dynamic viscosity of lubricating oil, υ_{Σ_p} is sum of tangential velocity at pitch point, $\rho_{red,p}$ is radius of curvature at pitch point.

Buckingham's empirical formula considered relative slide speed *Vs* (in/s), as Eq. (5).

$$\mu=0.05e^{-0.125V_s}+0.002\sqrt{V_s}\,. \tag{5}$$

Benedict & Kelly's empirical formula considered slide-roll ratio, maximum Hertzian contact stress, roughness, radius of curvature and elastic modulus, as Eq. (6).

$$\mu=0.0127\left(\frac{50}{50-S_{avg}}\right)\log_{10}\left[\frac{3.17\times10^8W'}{\eta_mV_sV_r^{\,2}}\right] \tag{6}$$

where, S_{avg} (μm) is roughness, W' (lbf/in) is time-varying load, V_r (in/s) is relative rolling speed.

Xu proposed a friction model based on EHL theory, and considered slide-roll ratio (*SR*), radius of curvature (*R*/m), maximum Hertzian contact stress (P_h/GPa), roughness (S_{avg}/μm) and elastic modulus (*E'*/GPa), as Eq. (7).

$$\mu=e^{f(SR,Ph,\eta_m,S_{avg})}P_h^{b2}|SR|^{b3}V_e^{b6}\eta_m^{b7}R^{b8} \tag{7}$$

where, $f(SR,P_h,\eta_m,S_{avg})$ is shown in Eq. (8).

$$f(SR,P_h,\eta_m,S_{avg})=b_1+b_4|SR|P_h\log_{10}(\eta_m)+b_5e^{-|SR|P_h\log_{10}(\eta_m)}+b_9e^{S_{avg}} \tag{8}$$

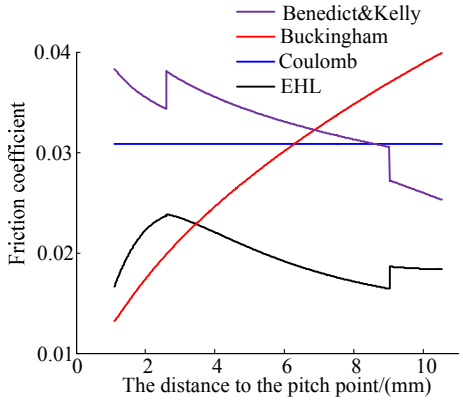

Fig. 8. The friction coefficient of GMBP.

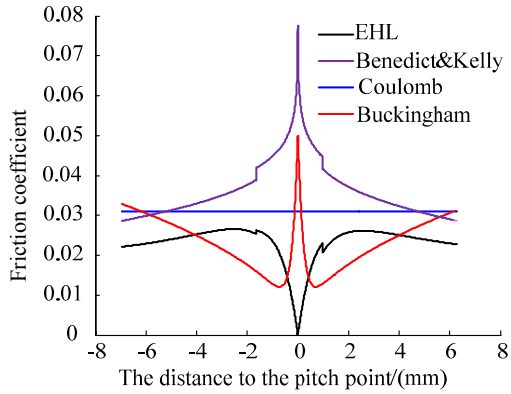

Fig. 9. The friction coefficient of OSG.

where, b_1~b_9 are listed in Table 2.

In order to compare different friction coefficient models, which are solved under the same condition, listed in Table 3.

The friction coefficients of the gear with meshing beyond pitch point and ordinary spur gear are solved. Results are shown in Figs. 8 and 9. Buckingham model do not consider time-varying load. Coulomb friction coefficient has friction coefficient of pitch point instead of itself, the GMBP isn't through pitch point, so Coulomb model does not apply in the GMNP. As the SR is zero at pitch point, friction coefficient is zero, but Benedict & Kelly model and Bucking model are maximum in Fig. 9, so these don't apply in the ordinary spur gear. The friction coefficient of the EHL theory is closer to real value by the proof of Xu's experiment. In this paper, the friction coefficient is solved by the EHL theory.

Comprehensive error ($e(t)$) includes eccentricity error and static transmission error of driving and driven gear. As is shown in Eq. (9).

$$e(t) = e\cos\omega t + e_p\cos(w_p t + \varphi_p) + e_g\cos(w_g t + \varphi_g) \tag{9}$$

where, e is static transmission error, which includes the tooth profile tooth curve error and pitch errors of gear, ω is meshing frequency, e_p is eccentricity error of driving gear, e_g is eccentricity error of driven gear, φ_p and φ_g is initial phase, respectively.

The equations of the system are derived in Eq. (10).

$$\begin{cases} m_p\ddot{x}_p + c_{px}\dot{x}_p + K_{px}f(x_p, b_{px}) = -F_{pi}\sin\alpha_t + f_{pi}\cos\alpha_t \\ m_p\ddot{y}_p + c_{py}\dot{y}_p + K_{py}f(y_p, b_{py}) = F_{pi}\cos\alpha_t + f_{pi}\sin\alpha_t \\ I_p\ddot{\theta}_p = T_p - F_{pi}(t)R_p - f_{pi}H_{pi} \\ m_g\ddot{x}_g + c_{gx}\dot{x}_g + K_{gx}f(x_g, b_{gx}) = F_{gi}\sin\alpha_t - f_{gi}\cos\alpha_t \\ m_g\ddot{y}_g + c_{gy}\dot{y}_g + K_{gy}f(y_g, b_{gy}) = -F_{gi}\cos\alpha_t - f_{gi}\sin\alpha_t \\ I_g\ddot{\theta}_g = T_g - F_{gi}(t)R_g - f_{gi}H_{gi}\,. \end{cases} \tag{10}$$

The composite DTE (dynamic transmission error), which is the relative dynamic displacement of driving pinion and driven gear along the LOA (line of action) direction, is defined as

$$\begin{aligned} \delta_{pg} = {} & (x_p - x_g)\cos(90-\alpha_t) + (y_p - y_g)\cos(180-\alpha_t) \\ & + R_p\theta_p + R_g\theta_g - e(\mathrm{t})\,. \end{aligned} \tag{11}$$

The normal forces acting on the driving pinion and driven gear are

$$F_{pi} = F_{gi} = c_m\dot{\delta}_{pg} + K_m f(\delta_{pg}, b)\,. \tag{12}$$

According to Ref. [16], clearance functions are derived as follow:

$$f(x_p,b_{px})=\begin{cases} x_p - b_{px} & x_p > b_{px} \\ 0 & -b_{px} < x_p < b_{px} \\ x_p + b_{px} & x_p < -b_{px} \end{cases} \quad f(y_p,b_{py})=\begin{cases} y_p - b_{py} & y_p > b_{py} \\ 0 & -b_{py} < y_p < b_{py} \\ y_p + b_{py} & y_p < -b_{py} \end{cases}$$

$$f(x_g,b_{px})=\begin{cases} x_g - b_{gx} & x_g > b_{gx} \\ 0 & -b_{gx} < x_g < b_{gx} \\ x_g + b_{gx} & x_g < -b_{gx} \end{cases} \quad f(y_g,b_{gy})=\begin{cases} y_g - b_{gy} & y_g > b_{gy} \\ 0 & -b_{gy} < y_g < b_{gy} \\ y_g + b_{gy} & y_g < -b_{gy} \end{cases}$$

$$f(\delta_{pg},b)=\begin{cases} x_{pg} - b & x_{pg} > b \\ 0 & -b < x_{pg} < b \\ x_{pg} + b & x_{pg} < -b\,. \end{cases} \tag{13}$$

As the order of magnitudes is large differences in equation, in order to get ideal answer, equation is nondimensionalized before solved. τ is dimensionless time, ω_n is natural frequency, Ω is meshing frequency, scale plate is b_c. K is average meshing stiffness.

$$\tau = \omega_n t \quad \omega_n = \sqrt{K/m_e} \quad \Omega = \omega/\omega_n \quad \Omega_p = \omega_p/\omega_n \quad \Omega_g = \omega_g/\omega_n$$

$$x = \bar{x}b_c \quad \dot{x} = \dot{\bar{x}}b_c\omega_n \quad \ddot{x} = \ddot{\bar{x}}b_c\omega_n^2 \quad b_c = 10^{-5}m \quad \overline{e(\tau)} = e(t)/b_c\omega_n^2\,. \tag{14}$$

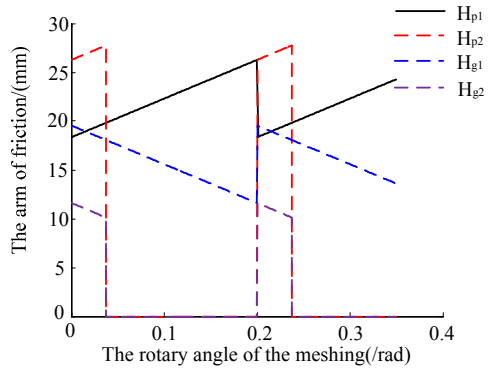

Fig. 10. The arm of friction.

The government equation is eliminated rigid displacement, results as follow:

$$\begin{cases} \ddot{\overline{x}}_p = -c_{px}\dot{\overline{x}}_p/m_p\omega_n - K_{px}f(\overline{x}_p,\overline{b}_{px})/m_p\omega_n^2 - (F_{pi}\sin\alpha_t - f_{pi}\cos\alpha_t)/b_c m_p\omega_n^2 \\ \ddot{\overline{y}}_p = -c_{py}\dot{\overline{y}}_p/m_p\omega_n - K_{py}f(\overline{y}_p,\overline{b}_{py})/m_p\omega_n^2 + (F_{pi}\cos\alpha_t + f_{pi}\sin\alpha_t)/b_c m_p\omega_n^2 \\ \ddot{\overline{x}}_g = -c_{gx}\dot{\overline{x}}_g/m_g\omega_n - K_{gx}f(\overline{x}_g,\overline{b}_{gx})/m_p\omega_n^2 + (F_{gi}\sin\alpha_t - f_{gi}\cos\alpha_t)/b_c m_g\omega_n^2 \\ \ddot{\overline{y}}_g = -c_{gy}\dot{\overline{y}}_g/m_g\omega_n - K_{gy}f(\overline{y}_g,\overline{b}_{gy})/m_g\omega_n^2 - F_{gi}\cos\alpha_t/m_g\omega_n^2 \\ \ddot{\overline{\delta}}_{pg} = (\ddot{\overline{x}}_p - \ddot{\overline{x}}_g)\sin\alpha_t + (\ddot{\overline{y}}_p - \ddot{\overline{y}}_g)\cos\alpha_t - \ddot{\overline{e}}(t) + (T_p - F_{pi}R_p - f_{pi}H_{pi})/b_c m_{ep}R_p\omega_n^2 + \ldots \\ \qquad (T_g - F_{pi}R_g - f_{gi}H_{gi})/b_c m_{eg}R_g\omega_n^2 \end{cases} \tag{15}$$

where, friction (f_{pi}) formula is shown in Eq. (16). f_1 and f_2 are friction coefficient of meshing point, λ is direction coefficient, if meshing point is located in front of pitch point , λ = -1, otherwise λ = 1. But actual meshing line is located in one side of the pitch point, is constant, in other words, meshing point is located in behind of pitch point in any time, λ = -1.

$$\begin{cases} f_{p1} = \lambda * f_1 * F_{p1} \\ f_{p2} = f_2 * F_{p2} \end{cases} \tag{16}$$

where $m_{ep} = I_p / R_p^2$, $m_{eg} = I_g / R_g^2$, and is rotational inertia, respectively. H_{pi} and H_{gi} is arm of friction, respectively, formulated as Eq. (17). The results are shown in Fig. 10.

$$\begin{cases} H_{p1} = PB_2 + R_p\omega_p \bmod(t,T) \\ H_{p1} = PB_2 + p_b + R_p\omega_p \\ H_{g1} = PG - H_{p1} \\ H_{g1} = PG - H_{p1} \end{cases} \\ \bmod(t,T),(\bmod(t,T) \le (chd-1)*T) \\ \bmod(t,T),(\bmod(t,T) \le (chd-1)*T)\,. \tag{17}$$

5. Results and analysis

The state of chaos and bifurcation are easy to cause noise and instability in gear transmission. It is necessary to study the effect of rotate speed, backlash, bearing clearance and damping on chaos and bifurcation. The bifurcation characteristics of dimensionless equivalent-displacement along the LOA (line of action) direction with changing rotate speed are shown in Figs. 11 and 12. The parameters of system are listed in Table 4.

Table 4. The condition parameters of system.

Power/(kW)	Damping ratio	Backlash/(μm)	Bearing clearance/(μm)
200	0.05	40	20

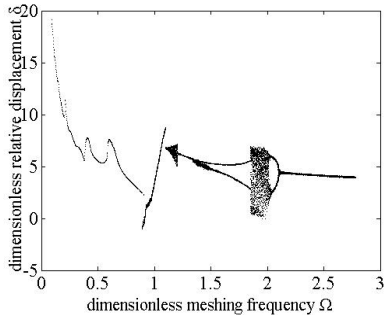

Fig. 11. The influence of speed on bifurcation characteristics is in the GMBP.

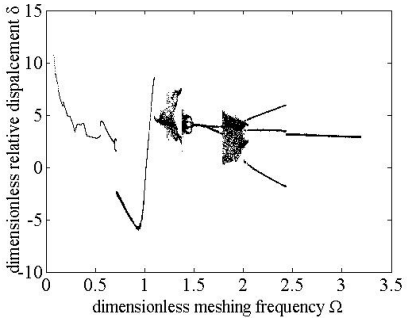

Fig. 12. The influence of speed on bifurcation characteristics is in the OSG.

From Figs. 11 and 12, the GMBP and OSG have similar state of motion in low speed range, rich bifurcation characteristics are shown with the rotate speed increases. The GMBP system of multiple clearance is from single-period to chaos by upheaval when Ω is 1.1. This characteristics is same to the OSG. The bifurcation behavior of GMBP and OSG has obvious differences after first natural frequency. The GMBP system is from chaos into quasi-periodic state at Ω = 1.2, system enters periodic-2 state at Ω = 1.45, while it's from periodic-2 to chaos when Ω is 1.9, from chaos to periodic-2 is at Ω = 2.05. The OSG system is from chaos into periodic-4 state at Ω = 1.45, it's from transient quasi-periodic to periodic-2 state at Ω = 1.75. The OSG system enters chaos state at Ω = 1.8. The GMBP system enters into single-period state by backward bifurcation when Ω is 2.15. But the OSG system enters three region chaos state by upheaval when dimensionless rotate speed is from 2.05 to 2.5. The OSG system enters into single-period state after Ω = 2.5.

As the gear system has inflicted a severe impact when the

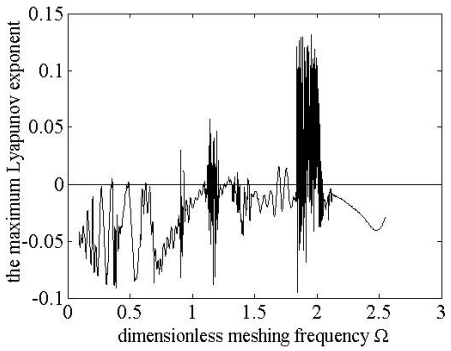

(a) The gear with meshing beyond pitch point

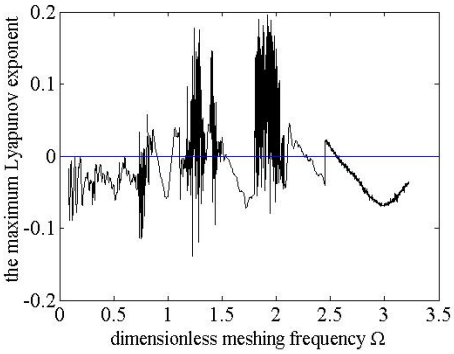

(b) The ordinary spur gear

Fig. 13. The maximum Lyapunov exponent with changing dimensionless frequency.

system is in chaos state, the chaos interval of the GMBP is smaller than the OSG. The amplitude of chaos interval of the GMBP is smaller than the OSG. Furthermore, periodicity stability of the GMBP is better than the OSG. The gear train with meshing beyond pitch point may lead to better vibration and noise.

In order to research the effect of bifurcation, the maximum Lyapunov exponent with changing dimensionless frequency is shown in Fig. 13. From the figures, if the maximum Lyapunov exponent is less zero, the system is period state, otherwise the system is chaos state. Besides the maximum Lyapunov exponent also contains points of less zero, it shows that chaos area also contains periodic window. Therefore, the accuracy of bifurcation figure is proved.

Chaos could destroy the gear train system badly, backlash is important factor of leading to chaos. The bifurcation characteristics of dimensionless equivalent-displacement along the LOA (line of action) direction with backlash are shown in Figs. 14 and 15. The parameters of system are listed in Table 5.

The bifurcation of gear train system is shown in Figs. 14 and 15. From the Fig. 14, range of single-period motion is between 0 and 2.2, gear train system experiences periodic-2 motion between 2.2 and 4.6, system enters chaos state when dimensionless backlash is 4.6, response enters periodic-5 when dimensionless backlash achieves 5.22, if dimensionless backlash is over 5.38, gear system will enter chaos state. From the

Table 5. The parameters of condition.

Power (kW)	Damping ratio	Dimensionless meshing frequency/Ω	Bearing clearance/(μm)
200	0.05	1.8	20

Table 6. The parameters of condition.

Power (kW)	Backlash/ (μm)	Dimensionless meshing frequency/Ω	Bearing clearance/(μm)
200	40	2.004	20

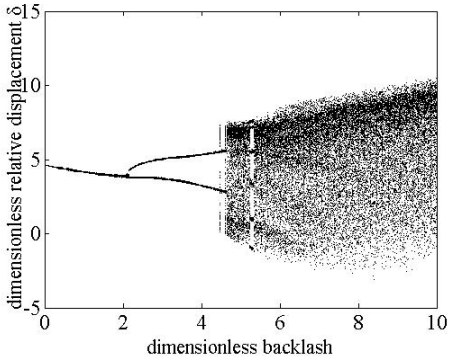

Fig. 14. The gear with meshing beyond pitch point.

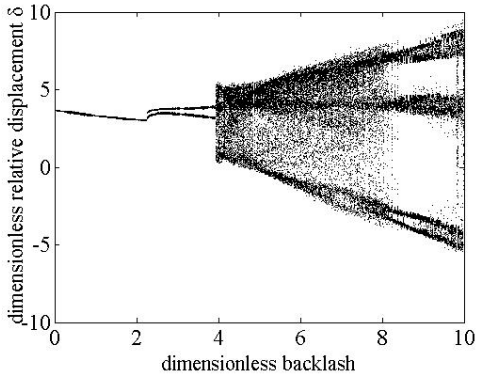

Fig. 15. The ordinary spur gear.

Fig. 15 range of single-period motion is between 0 and 2.3, gear system experiences periodic-2 motion between 2.3 and 4.0, system enters chaos state when dimensionless backlash is from 4.6 to 8.36. If dimensionless backlash is over 8.36, system will enter periodic-3 motion.

Backlash is an important factor of leading to chaos whether in the GMBP or OSG, the chaos interval of the GMBP is smaller than the OSG. It is necessary to choose appropriate backlash. Damping has been observed to be the main influencing factor that effects resonant region in gear system. The bifurcation behavior of dimensionless displacement of LOA is researched by variation of damping. The parameters of system are listed in Table 6.

From Figs. 16 and 17, the GMBP system is in chaos state in low damping ratio range. The GMBP system is from chaos

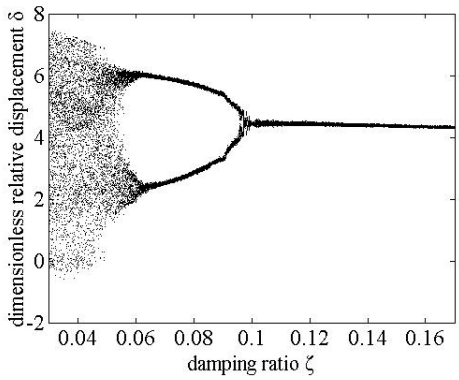

Fig. 16. The gear with meshing beyond pitch point.

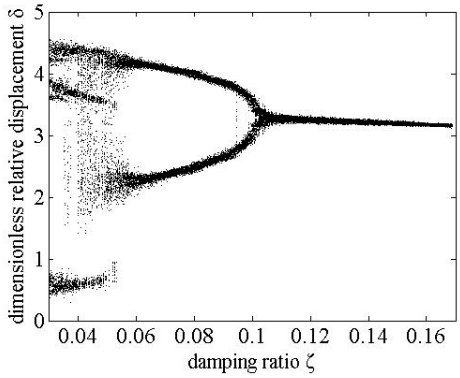

Fig. 17. The ordinary spur gear.

state to quasi-periodic motion by backward bifurcation between ζ = 0.061 and ζ = 0.101. The OSG system is from chaos state to quasi-periodic motion by back-ward bifurcation between ζ = 0.058 and ζ = 0.107. Dimensionless relative displacement diminishes with damping ratio, the OSG has the same characteristics. It is seen that damping may reduce chaotic strips whether in the GMBP or in the OSG.

The system motion changes from single-cycle motion to multi-cycle then to chaos due to the change of parameters. The change process of motion can be obtained through the bifurcation diagram of the system's motion state under these parameters. When the system appears in an unstable state, it can remain a stable state of motion by controlling the change of the parameters. This is actually the most useful and valuable place that can be reflected in the bifurcation diagram.

Bearing clearance has nonlinear characteristics, which may be a factor in bifurcation. It is necessary to study the effect of bearing clearance. The parameters of system are listed in Table 7.

The results are shown in Figs. 18 and 19. It is evident from Figs. 18 and 19 that the bifurcation behavior of gear system doesn't change with the bearing clearance. Although the OSG system is in periodic state when dimensionless bearing clearance is from 2.8 to 3.3, bearing clearance has less impact for system motion.

Table 7. The parameters of condition.

Power (kW)	Backlash /(μm)	Dimensionless meshing frequency/Ω	Damping ratio
200	40	1.107	0.05

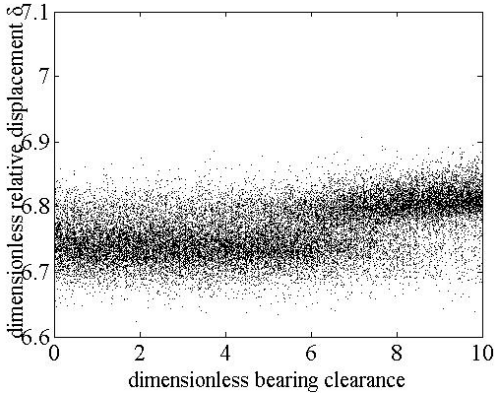

Fig. 18. The gear with meshing beyond pitch point.

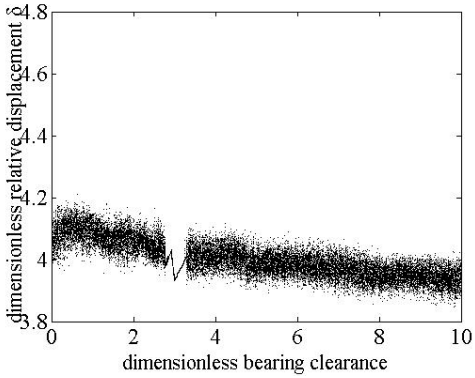

Fig. 19. The ordinary spur gear.

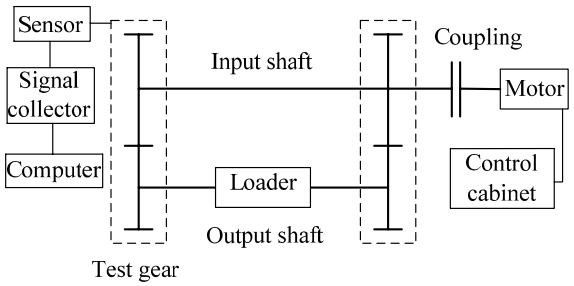

Fig. 20. Rig-layout.

6. Experiment and analysis

In order to prove accuracy of theory, the gear train system is experimented in the CL-100 test rig. Rig-layout is shown in Fig. 20.

The test platform arrangement is shown in Fig. 21. Sensor is placed on the input bearing cover, out-put bearing cover and base. Vibration is transmitted to collector by sense line. The

Table 8. The parameters of condition.

Condition	Torque/(N.m)	Rotate speed (GMBP) (r/min)	Rotate speed (OSG) /(r/min)	Bearing clearance/(μm)
1	62	750	703	1
2	85	750	703	1

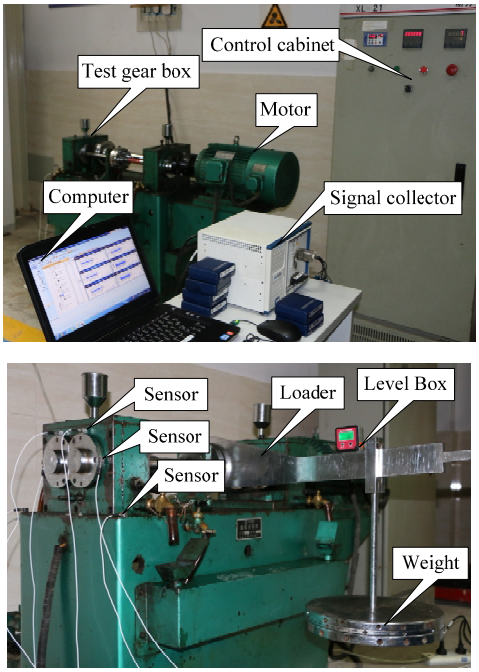

Fig. 21. CL-100 test rig.

angle formed by actual load and level direction, which is measured by the level box. Motor speed is controlled by the control cabinet. Load bears on the weight. Dynamic response is shown in computer. The assembling drawings of gear train of GMBP and OSG are shown in Fig. 22.

Since the backlash of gear isn't adjusted in the CL-100 test rig, the dynamic response between GMBP and OSG is verified at zero backlash. The condition parameters of system are listed in Table 8.

According to sampling theorem, sample frequency (f_s) and sample frequency (f_m) should meet the requirement $f_s \geq 2 f_m$, and in general, $f_s \geq 2.56$ fm, setting f_s = 5~10 f_m. According to meshing frequency, f_s is 4096 Hz, effective bandwidth (f_b) is 1600 Hz, sampling number (N_s) is 8192 and spectrum line numbers (N_1) is 3200 in the experiment. In order to prevent spectrum energy leaking, Han-ning-window is added.

The original frequency domain signal of vibration acceleration is shown from Figs. 23-26 in different conditions.

According to above diagrams, FDS contains meshing frequency, frequency doubling and other frequencies. So, the analysis results of theory haven't been verified. To get correct signal, the original frequency domain signal is processed by wavelet transform (WT). Without loss of generality, only driven-gear signal of conditon 1 has been analyzed and the results

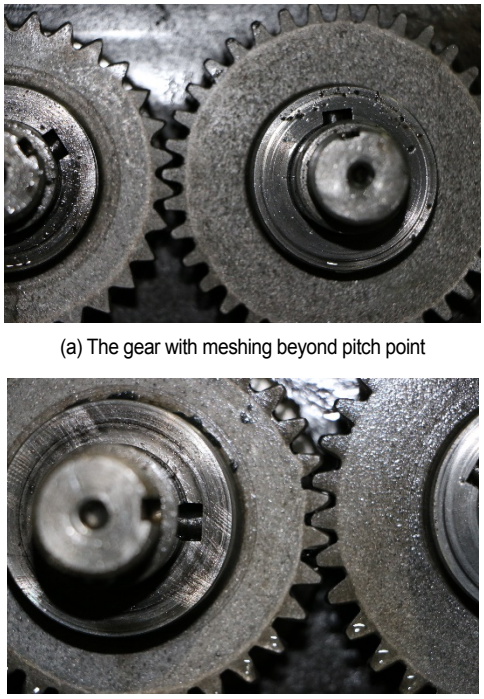

(a) The gear with meshing beyond pitch point

(b) The ordinary spur gear

Fig. 22. The assembling drawing of gear.

are shown from Figs. 27 and 28.

The experimental verifications test the original frequency domain signal of vibration acceleration, as shown in Figs. 23-28. From the figures, the following conclusions could be drawn: a) Vibration acceleration of gear system mainly reflects meshing frequency and double meshing frequency. b) Vibration acceleration of GMBP is smaller than vibration acceleration of OSG. c) Meshing frequency has main impact on vibration acceleration of OSG and double meshing frequency has main impact on vibration acceleration of GMBP.

The frequency domain signal has been transformed into time domain signal by WT, and results are shown in Figs. 29 and 30.

According to the figures, the conclusion could be drawn that vibration acceleration of OSG is smaller than vibration acceleration of GMBP whether X direction or Y direction.

The vibration accelerations calculated with numerical simulation of the system is shown in Figs. 31 and 32.

From the figures, the vibration acceleration is calculated, which is similar to result measured by test. The vibration acceleration of GMBP is smaller than OSG in time domain. Vibration acceleration of Y direction is only analyzed. The time domain signal is transformed into frequency domain signal by FFT, which is shown in Fig. 33.

According to Fig. 33, the following conclusions could be drawn: a) Magnitude of acceleration calculated with theoretical is similar to test value. b) From magnitude, the GMBP-driven is smaller than OSG. c) Meshing frequency has main impact on vibration acceleration of OSG and double meshing frequency has mainly impact on vibration acceleration of GMBP.

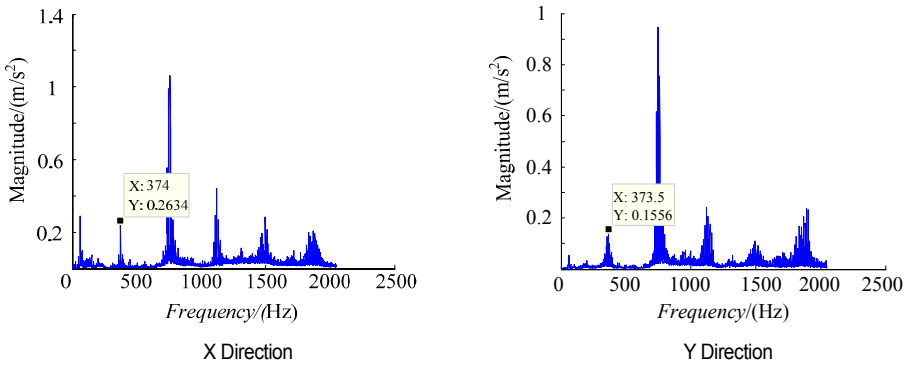

Fig. 23. The frequency domain signal (condition 1) of GMBP-driven.

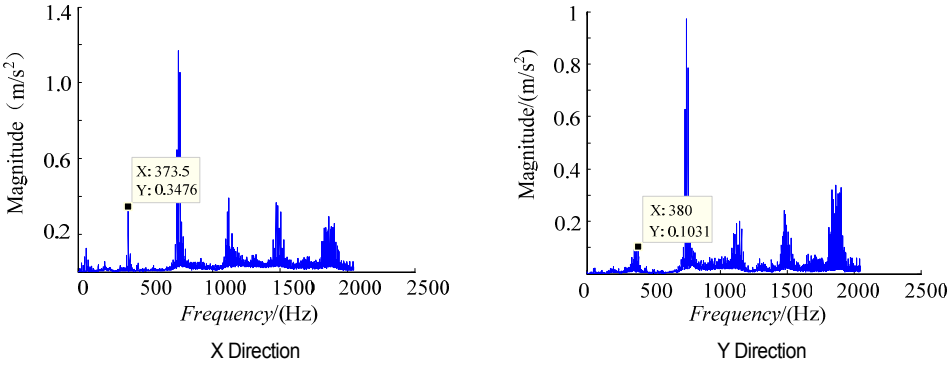

Fig. 24. The frequency domain signal (condition 2) of GMBP-driven.

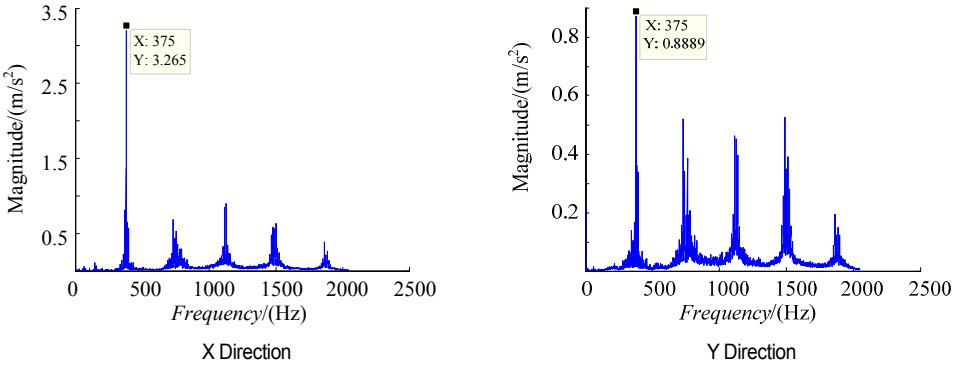

Fig. 25. The frequency domain signal (condition 1) of OSG-driven.

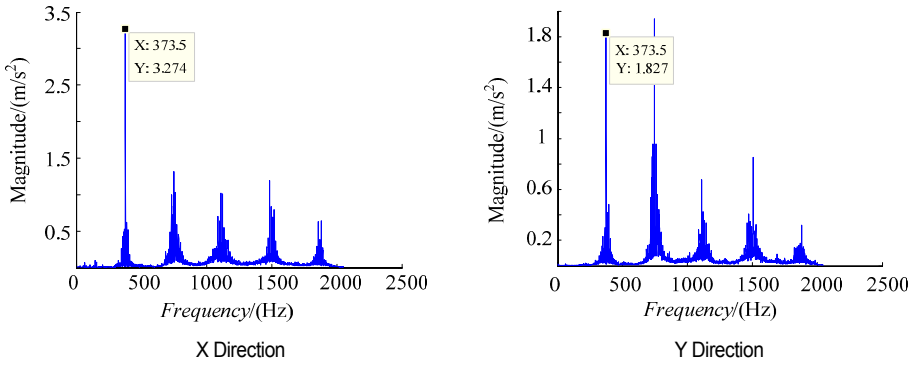

Fig. 26. The frequency domain signal (condition 2) of OSG-driven.

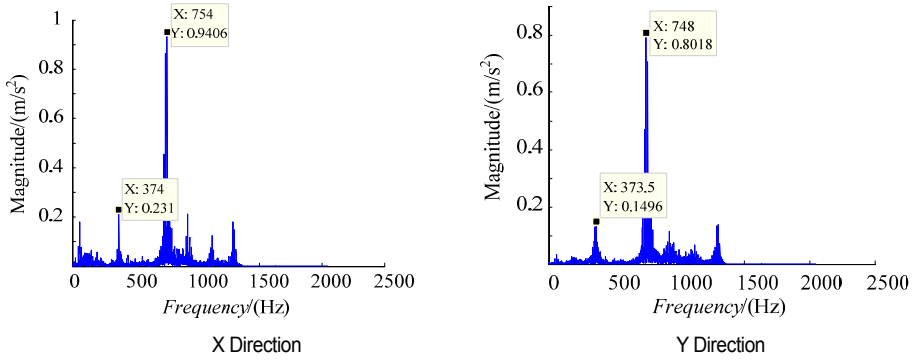

Fig. 27. The frequency domain signal of GMBP-driven.

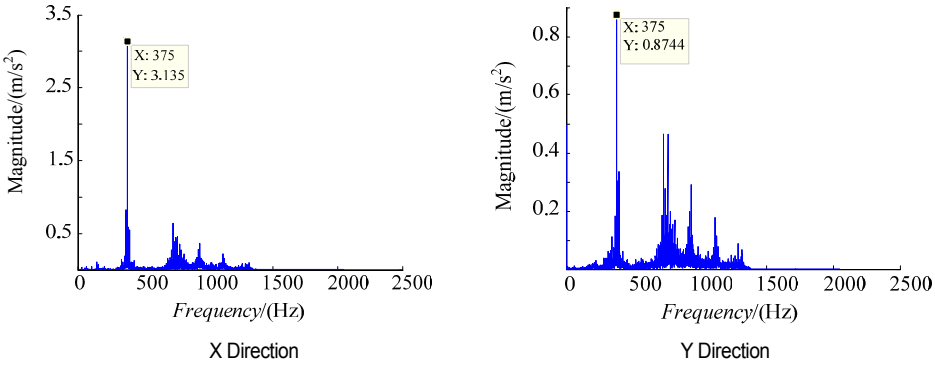

Fig. 28. The frequency domain signal of OSG-driven.

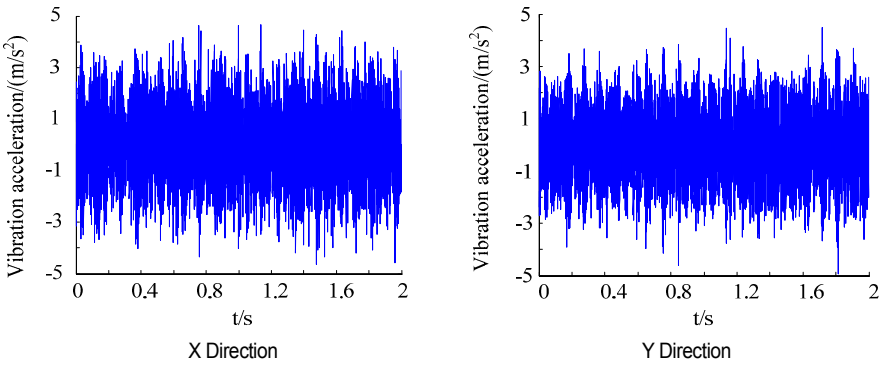

Fig. 29. The time domain signal of GMBP-driven.

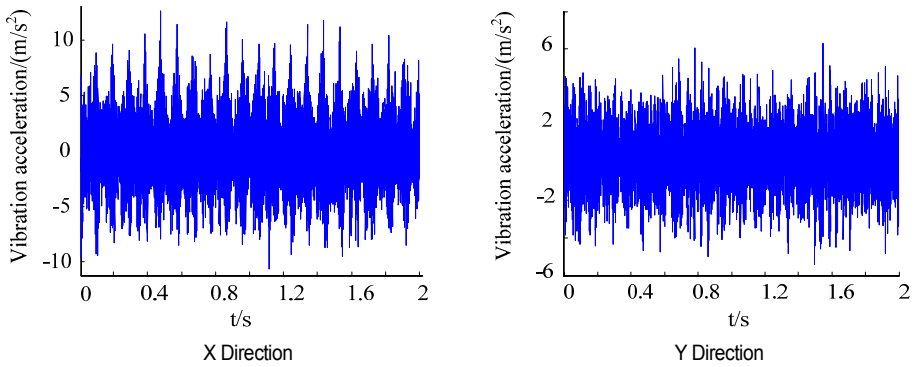

Fig. 30. The time domain signal of OSG-driven.

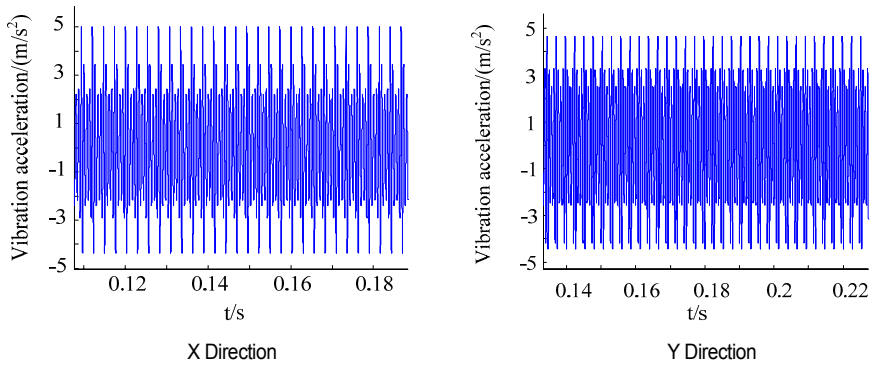

Fig. 31. The time domain signal of GMBP-driven.

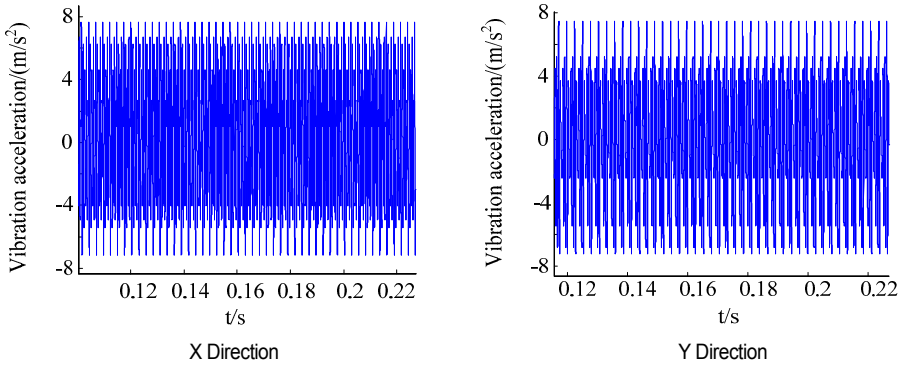

Fig. 32. The time domain signal of OSG-driven.

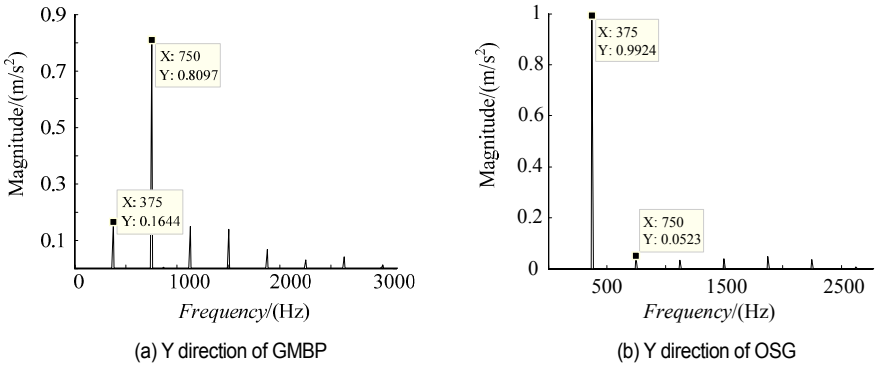

Fig. 33. The frequency domain signal.

7. Conclusion

In this paper, an external gear system with meshing beyond pitch point and an external ordinary gear system are set as the research target, and the global bifurcation characteristics caused by input speed, backlash, damping and bearing clearance were investigated. First, the gear parameters were optimized by objective function of minimum mass. Second, the stiffness of the external gears with meshing beyond pitch point considering gear wheel body deformation is computed by using material mechanics method, which is similar with the Fourier series method. Third, the load distribution among teeth is calculated. Fouth, friction coefficient of tooth surface is solved by Benedict & Kelly model, Buckingham model, Coulomb model and EHL model. Fifth, the global bifurcation characteristics are compared and analyzed by Matlab. Sixth, the global bifurcation characteristics are researched by the maximum Lyapunov exponent. Finally, the vibration acceleration is measured by test and calculated by Matlab.

From this paper, we can draw the following conclusions: a) It is evident from bifurcation diagrams that bearing clearance and backlash lead to chaos in dynamic of gear system, and backlash is the major factor. Damping may reduce chaotic strips. Gear system will enter chaos state when the backlash increases. b) The amplitude of chaos interval of the GMBP is smaller than the OSG. Furthermore, periodicity stability of the

GMBP is better than the OSG. Therefore, the gear with meshing beyond pitch point may lead to better vibration and noise. c) Vibration acceleration of GMBP is smaller than vibration acceleration of OSG. Meshing frequency has main impact on vibration acceleration of OSG and double meshing frequency has main impact on vibration acceleration of GMBP.

Based on the above, one can draw a conclusion that gear system with meshing beyond pitch will leads to better vibration performance than ordinary gear train.

Acknowledgments

This study was supported by National Key Laboratory of Science and Technology on Helicopter Transmission (Nanjing University of Aeronautics and Astronautics) (Grant No. HTL-A-19K03) and the National Natural Science Foundation of China (51975274).

References

[1] R. F. Li and J. J. Wang, *The Dynamics of Gear System*, Science Press (1997).

[2] P. Velex and P. Sainsot, An analytical study of tooth of tooth friction excitations in spur and helical gears, *Mechanism and Machine Theory*, 37 (7) (2002) 641-648.

[3] M. Vaishya and R. Houser, Modeling and analysis of sliding friction in gear dynamics, *Proceedings of the 2000 ASME Design Engineering Technical Conferences*, Baltimore, USA: DETC 2000/PTG-14430 (2000) 601-610.

[4] M. Vaishya and R. Houser, Sliding friction induced non-linearity and parametric effects in gear dynamics, *Journal of Sound and Vibration*, 248 (4) (2001) 671-694.

[5] S. He, R. Gunda and R. Singh, Inclusion of sliding friction in contact dynamics model for helical gears, *Journal of mechanical Design*, 129 (1) (2007) 48-57.

[6] S. He, S. Cho and R. Singh, Prediction of dynamic friction forces in spur gears using alternate sliding friction formulations, *Journal of Sound and Vibration*, 309 (3-5) (2008) 843-851.

[7] J. Y. Tang, S. Y. Chen and J. Zhong, A improved nonlinear model for a spur gear pair system, *Engineering Mechanics*, 25 (1) (2008) 217-223.

[8] E. Buckingham, *Analytical Mechanics of Gears*, McGraw-Hill Book Company, New York (1949).

[9] J. Zhang et al., Dynamic analysis for spur gears considering friction effect, *Journal of Vibration and Shock*, 31 (12) (2012) 126-132.

[10] Y. Z. Sun, R. P. Zhu and H. Y. Bao, Calculation of mean friction coefficient in scuffing strength for gear drive with meshing beyond pitch point, *Journal of Aerospace Power*, 28 (9) (2013) 2514-2160.

[11] T. J. Li et al., Stability of motion state and bifurcation properties of planetary gear train, *Journal of Central South University*, 19 (2012) 1543-1547.

[12] J. Y. Tang et al., Effect of static transmission error on dynamic responses of spiral bevel gears, *Journal of Central South University*, 20 (2013) 640-647.

[13] A. Farshidianfar and A. Saghafi, Bifurcation and chaos prediction in nonlinear gear systems, *Shock and Vibration* (2014) 809739.

[14] C. W. Chang-Jian and S. M. Chang, Bifurcation and chaos analysis of spur gear pair with and without nonlinear suspension, *Nonlinear Analysis Real World Applications*, 12 (2) (2011) 979-989.

[15] C. F. Li et al., Vibration of bending-torsion coupling gear-rotor rolling bearing transmission system, *Journal of Aeronautical Power*, 29 (7) (2014) 1543-1555.

[16] D. P. Sheng et al., Bifurcation characteristic and modeling of transvers-torsional spur gear vibration considering friction and multiple clearances, *Journal of Aeronautical Power*, 30 (2) (2015) 498-506.

[17] T. M. Xiang et al., Experimental modal test of the spiral bevel gear wheel using the PolyMAX method, *Journal of Mechanical Science and Technology*, 32 (1) (2018) 21-28.

[18] R. B. Chen, J. X. Zhou and W. L. Sun, Dynamic characteristics of a planetary gear system based on contact status of the tooth surface, *Journal of Mechanical Science and Technology*, 32 (1) (2018) 69-80.

[19] J. Yu et al., Fault diagnosis of planetary gearbox with incomplete information using assignment reduction and flexible naive Bayesian classifier, *Journal of Mechanical Science and Technology*, 32 (1) (2018) 37-47.

[20] Y. Y. Zhang, H. Y. Bao and L. L. Li, Nonlinear dynamic analysis of an external gear system with meshing beyond pitch point, *Proceedings of the International Conference on Power Transmissions* (2016).

[21] X. L. Zhu and Z. K. E, *Analysis of Load Capacity of Gears*, Beijing Education Publishing House, Beijing (1992).

He-yun Bao received her Ph.D. degree in Mechanical Engineering in Nanjing University of Aeronautics and Astronautics (NUAA) in 2007. She was a visiting scholar at University of Virginia (UVA) from 2015 to 2016. She is currently an Associate Professor of the National Key Laboratory of Science and Technology on Helicopter Transmission, NUAA. Her research interests are focused on helicopter transmission system, gear dynamics, rotor dynamic analysis, dynamic modelling , numerical simulations and thermal analysis.